PERGAMON

International Journal of Solids and Structures 39 (2002) 2707–2730

INTERNATIONAL JOURNAL OF SOLIDS and STRUCTURES

www.elsevier.com/locate/ijsolstr

Special virtual fields for the direct determination of material parameters with the virtual fields method. 2—Application to in-plane properties

Michel Grédiac [a,*], Evelyne Toussaint [a], Fabrice Pierron [b]

[a] *Laboratoire d'Etudes et de Recherches en Mécanique des Structures, Université Blaise Pascal Clermont II, 24, avenue des Landais, BP 206, 63174 Aubière Cedex, France*

[b] *Laboratoire de Mécanique et Procédés de Fabrication, Ecole Nationale Supérieure des Arts et Métiers, rue Saint-Dominique, BP 508, 51006 Châlons-en-Champagne Cedex, France*

Abstract

This paper deals with the direct identification of mechanical parameters that govern the in-plane constitutive law of orthotropic materials. Those parameters are extracted from heterogeneous strain fields that occur in a short beam specimen tested in a Iosipescu fixture. The procedure used is the virtual fields method with special virtual fields. The case of linear elasticity is first addressed. It is shown that the parameters are directly extracted with this method: no iterative calculations are required. The stability is also discussed in different cases. A non-linear shear response is then considered. The parameter that governs this non-linearity is also directly identified with the special virtual fields.

Keywords: Material parameters; Orthotropic; Linear elasticity; Non-linearity

1. Introduction

The determination of stiffness parameters for anisotropic materials like composites is more complicated than for isotropic materials: the number of parameters is higher and difficulties in obtaining homogeneous strain fields give rise to some problems in the experimental procedures. A promising way for a better measurement of those parameters consists in performing unusual tests that give rise to non-uniform strain fields. All the unknown parameters are expected to be involved in the strain field: they can therefore be identified if a suitable strategy is used since no closed-form solution is generally available. Extracting the stiffness parameters from natural frequencies of vibrating plates is one of the most popular procedures (Ayorinde and Gibson, 1993; Deobald and Gibson, 1988; Mota Soares et al., 1993; Araujo et al., 1996; Frederiksen, 1997; Cunha and Piranda, 1999; Okada et al., 1999). Extracting the parameters from heterogeneous strain fields that occur in static tests has been also proposed in the literature (Prabhakaran and

* Corresponding author. Tel.: +33-4-73-40-75-29; fax: +33-4-73-40-74-94.
E-mail address: grediac@lermes.univ-bpclermont.fr (M. Grédiac).

0020-7683/02/$ - see front matter
PII: S0020-7683(02)00128-2

Chermahini, 1984; Hendricks, 1991; Grédiac, 1989). In this last work, it is proposed to process the measured data with a particular use of the principle of virtual work. This global equilibrium is written with specific virtual fields, allowing the determination of the stiffness parameters. During the last decade, this approach has been successfully used in different cases of anisotropic material characterization (see for instance Grédiac and Vautrin (1990), Grédiac (1996a,b), Grédiac and Pierron (1998), Grédiac et al. (1999), Pierron et al. (2000), Pierron and Grédiac (2000) and Grédiac et al. (2002)). In the above studies, the virtual fields were however determined intuitively since no general procedure for constructing them was available. The users of the method were therefore not sure to process the measured fields with optimized virtual fields in terms of accuracy and stability of the identified parameters. A dramatic improvement is proposed in a companion paper (Grédiac et al., 2002) in which it is proposed to construct automatically special virtual fields that directly provide the unknown parameters. The question of finding the virtual fields can then be solved by using a program that automatically builds them.

The present paper focuses on some of the computational aspects of the virtual fields method with special virtual fields in the case of orthotropic in-plane properties. The principle of the construction of the special virtual fields is recalled in the first part of the paper. Numerical simulations are then carried out to assess the accuracy and the stability of the procedure. It is shown that an infinity of special virtual fields can be found for each parameter. A procedure is proposed to select the *optimized* virtual fields which are the less sensitive to noisy data. Such fields provide optimized identified values for the parameters. Finally, the capability of the procedure for identifying the parameter that governs a non-linear shear response is addressed.

2. Special virtual fields for finding the four stiffnesses of an orthotropic law

Let us consider a specimen of any shape subjected to an in-plane loading (see Fig. 1). V, S and e are respectively the volume, the external surface and the thickness of the specimen. The case of an orthotropic

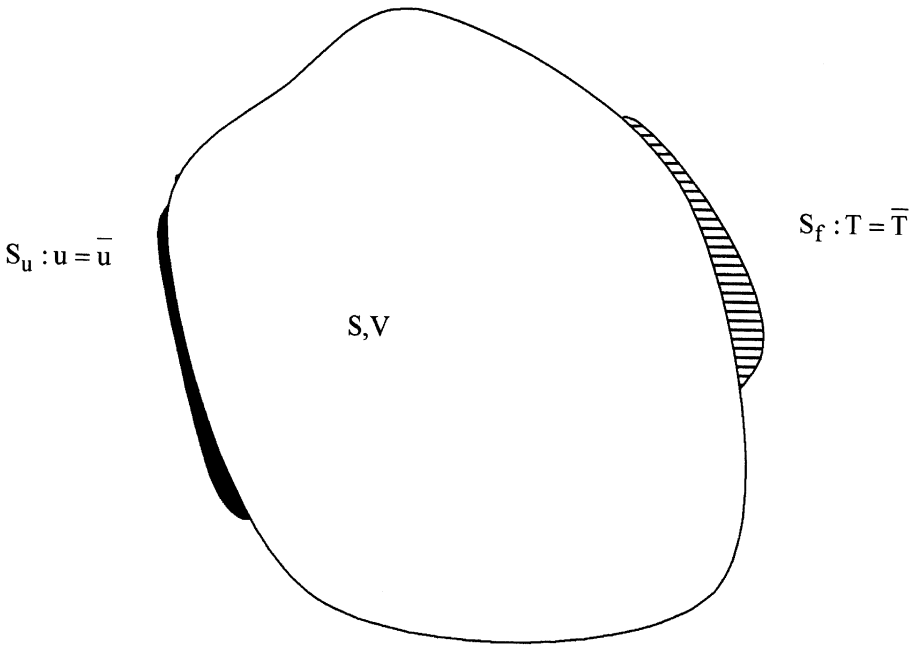

Fig. 1. Plate of any shape under in-plane loading.

elastic linear relationship is considered here for the sake of simplicity, but it must be pointed out that a complete anisotropic law with six unknowns could be investigated with the same procedure (Grédiac et al., 2002). In the same way, any non-linearity such that the stress/strain relationship may be written as a polynomial could also be investigated with the same procedure (Grédiac et al., 2002), as illustrated below through an example. In the orthotropy axes, the stress/strain relations may be written as (with the usual rule of contracted indices: $xx \to x$, $yy \to y$, $xy \to s$)

$$\begin{bmatrix} \sigma_x \\ \sigma_y \\ \sigma_s \end{bmatrix} = \begin{bmatrix} Q_{xx} & Q_{xy} & 0 \\ Q_{xy} & Q_{yy} & 0 \\ 0 & 0 & Q_{ss} \end{bmatrix} \begin{bmatrix} \epsilon_x \\ \epsilon_y \\ \epsilon_s \end{bmatrix} \tag{1}$$

The goal is here to identify Q_{xx}, Q_{yy}, Q_{xy} and Q_{ss} from the heterogeneous strain/stress fields that take place in the specimen and for which no closed-form solution for the actual displacement and strain fields are available. The global equilibrium of the specimen may be written as

$$\int_V \sigma : \epsilon^* \, \mathrm{d}V = \int_{S_f} \mathbf{T}\mathbf{u}^* \, \mathrm{d}S \tag{2}$$

Feeding the stress/strain relationship (1) in the above equation leads to

$$I_{xx}Q_{xx} + I_{yy}Q_{yy} + I_{xy}Q_{xy} + I_{ss}Q_{ss} = \int_{S_f} T_i u_i^* \, \mathrm{d}S \tag{3}$$

with

$$\begin{cases} I_{xx} = e \int_S \epsilon_x \epsilon_x^* \, \mathrm{d}S \\ I_{yy} = e \int_S \epsilon_y \epsilon_y^* \, \mathrm{d}S \\ I_{xy} = e \int_S (\epsilon_x \epsilon_y^* + \epsilon_y \epsilon_x^*) \, \mathrm{d}S \\ I_{ss} = e \int_S \epsilon_s \epsilon_s^* \, \mathrm{d}S \end{cases} \tag{4}$$

The basic idea of the virtual fields method consists in writing Eq. (3) with different particular virtual fields $\mathbf{u}^*$, ϵ^* (Grédiac, 1989). If as many different virtual fields as unknown parameters are found, a linear system is obtained and inverted to get the unknowns.

One of the key-points of the method is the choice of the virtual fields since one has to choose among an infinite number of possibilities. In the above references, those fields were chosen intuitively or following some empirical rules. For instance, the virtual fields were such that some components in the matrix of the linear system were zero. Then the linear equations were partially uncoupled. In a companion paper (Grédiac et al., 2002), it is shown that some virtual fields called *special* virtual fields render the matrix of linear system equal to unity, leading therefore to a direct identification of the unknown parameters. These special virtual fields are denoted hereafter $\hat{\mathbf{u}}^*$, $\hat{\epsilon}^*$. The idea is to use the principle of virtual work with those special virtual fields such that three of the four I_{ij}'s are zero whereas the fourth one is equal to 1 m^3. This leads to a direct determination of the parameter which coefficient is 1 in Eq. (3). Since four material parameters are to be determined, the problem is to find four special virtual fields $\hat{\mathbf{u}}^{*(\mathbf{i})}$, $\mathbf{i} = \mathbf{1}, \ldots, \mathbf{4}$ such that

$$\begin{cases} \text{with } \hat{\mathbf{u}}^{*(\mathbf{1})} : \; I_{xx} = 1, \; I_{yy} = I_{xy} = I_{ss} = 0 \quad \text{and} \quad Q_{xx} = \int_{S_f} T_i \hat{u}_i^{*(1)} \, \mathrm{d}S \\ \text{with } \hat{\mathbf{u}}^{*(\mathbf{2})} : \; I_{yy} = 1, \; I_{xx} = I_{xy} = I_{ss} = 0 \quad \text{and} \quad Q_{yy} = \int_{S_f} T_i \hat{u}_i^{*(2)} \, \mathrm{d}S \\ \text{with } \hat{\mathbf{u}}^{*(\mathbf{3})} : \; I_{xy} = 1, \; I_{xx} = I_{yy} = I_{ss} = 0 \quad \text{and} \quad Q_{xy} = \int_{S_f} T_i \hat{u}_i^{*(3)} \, \mathrm{d}S \\ \text{with } \hat{\mathbf{u}}^{*(\mathbf{4})} : \; I_{ss} = 1, \; I_{xx} = I_{yy} = I_{xy} = 0 \quad \text{and} \quad Q_{ss} = \int_{S_f} T_i \hat{u}_i^{*(4)} \, \mathrm{d}S \end{cases} \tag{5}$$

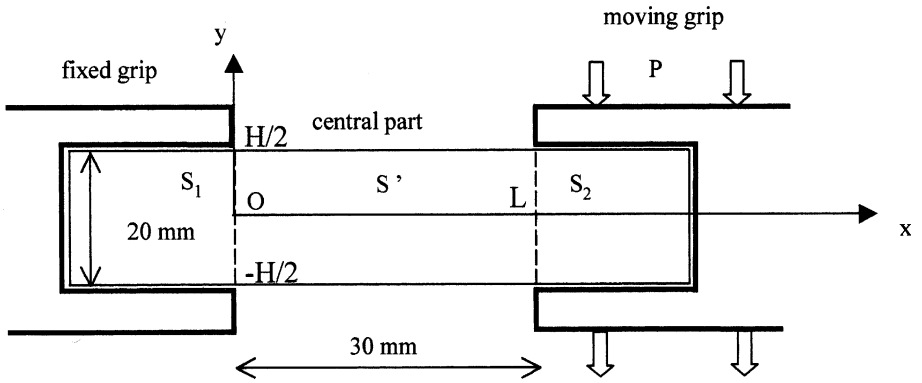

Fig. 2. Tested specimen.

In each case, the unknown parameter is equal to the virtual work of the applied loading. $\hat{\mathbf{u}}^{*(1)}$ directly provides Q_{xx}, $\hat{\mathbf{u}}^{*(2)}$ directly provides Q_{yy}, $\hat{\mathbf{u}}^{*(3)}$ directly provides Q_{xy} and $\hat{\mathbf{u}}^{*(4)}$ directly provides Q_{ss}.

In Ref. Grédiac et al. (2002), a general procedure for constructing the special virtual fields is proposed. The aim is here to examine the practical implementation of this procedure for a particular testing configuration: a short beam in a Iosipescu fixture (see Fig. 2). Such a configuration can be tested in practice with a suitable testing device (Pierron and Vautrin, 1994). Heterogeneous strain/stress fields take places in the central part S' of the specimen and no closed-form solution is available. Previous work on this geometry has been recently carried out (Pierron and Grédiac, 2000; Grédiac et al., 2001), but the virtual fields were found intuitively and one could not find uncoupled equations in the principal matrix of the linear system. The objective is here to test the capability of the method for finding automatically the special virtual fields.

3. Construction of the special virtual fields

3.1. Constraints under which the special virtual fields must be built

Let us now examine the properties that must satisfy the special virtual fields $\hat{\mathbf{u}}^*$ to be determined. As explained in Ref. Grédiac et al. (2002), those fields must obey three conditions. Two extra conditions must also be satisfied if only one part of the actual strain field is measured. The three first conditions are

- *Condition 1:* The special virtual fields must be kinematically admissible. Hence,

$$\forall M \in S_u, \quad \hat{\mathbf{u}}^*(M) = \mathbf{0} \tag{6}$$

- *Condition 2:* For each unknown stiffness, the special virtual fields must verify the four fundamental equalities in Eq. (5). For instance, $\hat{\mathbf{u}}^{*(1)}$ is such that the first four equalities in Eq. (5) are verified.
- *Condition 3:* In general, only the resulting force along the vertical direction is known but the distribution of the applied loading remains unknown. Then the special virtual fields must be such that the virtual displacement of S_f is vertical and constant. Hence the virtual work of the applied load is simply the value of the resulting force multiplied by this constant.

In the present case, it is assumed that the actual strain field is known over the central part S' of S only. Such a case arises in practice when a CCD camera is used and captures only a part of the actual strain field. Then, two additional conditions must also be verified in this case:

- *Condition 4:* The special virtual fields must only give rise to non-zero virtual strain components inside S' and must be solid-rigid like outside S' (i.e. they must give rise to zero virtual strain components outside S').
- *Condition 5:* The special virtual fields must be continuous along the boundary between S_1 and S' as well as between S_2 and S'.

Let us now examine the automatic construction of the special virtual fields through the use of the five above conditions.

3.2. Right-hand side grip

3.2.1. Condition 4

Condition 4 must be verified. The virtual field must therefore be solid-rigid like over S_2. Then, the virtual strain field satisfies

$$\begin{cases} \hat{\epsilon}_x^*(M) = 0 \\ \hat{\epsilon}_y^*(M) = 0 \quad \forall M \in S_2 \\ \hat{\epsilon}_s^*(M) = 0 \end{cases} \tag{7}$$

The virtual displacement field is deduced by integration

$$\begin{cases} \hat{u}_x^*(M) = ay + b \\ \hat{u}_y^*(M) = -ax + c \quad \forall M \in S_2 \end{cases} \tag{8}$$

where a, b and c are constants.

3.2.2. Condition 3

After condition 3, the virtual displacement of S_f must be vertical only. Since it has been shown above that the virtual displacement over S_2 is solid-rigid like, it is a trivial matter to see that a, b and c must satisfy

$$a = 0, \quad b = 0, \quad c \neq 0 \tag{9}$$

Consequently, the whole part S_2 is subjected to a virtual vertical translation.

3.3. Left-hand side grip

3.3.1. Condition 4

Condition 4 must be satisfied. The virtual field must therefore be solid-rigid like over S_1 (see Fig. 2). Then, the virtual strain field satisfies

$$\begin{cases} \hat{\epsilon}_x^*(M) = 0 \\ \hat{\epsilon}_y^*(M) = 0 \quad \forall M \in S_1 \\ \hat{\epsilon}_s^*(M) = 0 \end{cases} \tag{10}$$

The virtual displacement field is deduced by integration

$$\begin{cases} \hat{u}_x^*(M) = a'y + b' \\ \hat{u}_y^*(M) = -a'x + c' \quad \forall M \in S_1 \end{cases} \tag{11}$$

where a', b' and c' are constants.

3.3.2. Condition 3

After condition 3, the virtual displacement of the contact line between the specimen and the left-hand side grip must be 0. Since it has been shown above that the virtual displacement over S_1 must be solid-rigid like, it is a trivial matter to see that a', b' and c' must satisfy

$$a' = 0, \quad b' = 0, \quad c' = 0 \tag{12}$$

Consequently, the left-hand side grip does not virtually move.

3.4. Central part S'

3.4.1. Condition 5

Since the special virtual field must be continuous between S' and S_2, the virtual horizontal displacement must be zero at the boundary between S' and S_2 (see Fig. 2)

$$\hat{u}_x^*(L,y) = 0 \quad \forall y \in \left[-\frac{h}{2}, \frac{h}{2}\right] \tag{13}$$

For the same reason, the vertical displacement must be constant along this boundary

$$\hat{u}_y^*(L,y) = \text{constant} \quad \forall y \in \left[\frac{-h}{2}, \frac{h}{2}\right] \tag{14}$$

which implies

$$\hat{\epsilon}_y^*(L,y) = 0 \quad \forall y \in \left[\frac{-h}{2}, \frac{h}{2}\right] \tag{15}$$

In the same way, since the special virtual field must be continuous between S' and S_1, the virtual horizontal and vertical displacements must be zero along the boundary between S' and S_1.

$$\hat{u}_x^*(0,y) = \hat{u}_y^*(0,y) = 0 \quad \forall y \in \left[-\frac{h}{2}, \frac{h}{2}\right] \tag{16}$$

3.4.2. Condition 2

The explicit form of the virtual displacement field must be known to determine the virtual strain field and the equations deduced from condition 2. The aim of the following section is therefore to propose a general expression for the special virtual displacement field.

3.5. Choice of a basis and general expression of the virtual fields

According to Ref. Grédiac et al. (2002), it is proposed to write the special virtual displacement fields in the central part S' as follows

$$\begin{cases} \hat{u}_x^* = \frac{x(x-L)}{L^2}\left(\sum_{i=0}^{m}\sum_{j=0}^{n} A_{ij}\left(\frac{x}{L}\right)^i\left(\frac{y}{H}\right)^j\right) \\ \hat{u}_y^* = \frac{x}{L}\left(\sum_{i=0}^{p}\sum_{j=0}^{q} B_{ij}\left(\frac{x}{L}\right)^i\left(\frac{y}{H}\right)^j\right) \end{cases} \tag{17}$$

where the A_{ij}'s and the B_{ij}'s are coefficients given in m. It can be checked that the conditions in Eqs. (13)–(16) are verified with such a choice. Eq. (15) leads to

$$\hat{\epsilon}_y^*(L,y) = \left(\sum_{i=0}^{p} \sum_{j=1}^{q} jB_{ij} \left(\frac{y}{H} \right)^{j-1} \right) = 0 \quad \forall y \in \left[\frac{-h}{2}, \frac{h}{2} \right] \tag{18}$$

since this equality must be satisfied $\forall y \in \left[\frac{-h}{2}, \frac{h}{2}\right]$. Then, we can write

$$\sum_{i=0}^{p} B_{ij} = 0 \quad \forall j \in [1,q] \tag{19}$$

Hence, we obtain q linear equations where the B_{ij}'s are the unknowns. These q linear equations must be added to the four provided by condition 2.

3.6. Equations provided by condition 2 and final linear system

The special virtual strain components are easily deduced by differentiation of the special virtual displacement field

$$\begin{cases} \hat{\epsilon}_x^* = \frac{2x-L}{L^2} \left(\sum_{i=0}^{m} \sum_{j=0}^{n} A_{ij} \left(\frac{x}{L} \right)^i \left(\frac{y}{H} \right)^j \right) + \frac{x(x-L)}{L^2} \left(\sum_{i=1}^{m} \sum_{j=0}^{n} iA_{ij} \left(\frac{x}{L} \right)^{i-1} \left(\frac{y}{H} \right)^j \right) \\ \hat{\epsilon}_y^* = \frac{x}{L} \left(\sum_{i=0}^{p} \sum_{j=1}^{q} jB_{ij} \left(\frac{x}{L} \right)^i \left(\frac{y}{H} \right)^{j-1} \right) \\ \hat{\epsilon}_s^* = \frac{x(x-L)}{L^2} \left(\sum_{i=0}^{m} \sum_{j=1}^{n} jA_{ij} \left(\frac{x}{L} \right)^i \left(\frac{y}{H} \right)^{j-1} \right) + \frac{1}{L} \left(\sum_{i=0}^{p} \sum_{j=0}^{q} B_{ij} \left(\frac{x}{L} \right)^i \left(\frac{y}{H} \right)^j \right) + \frac{x}{L} \left(\sum_{i=1}^{p} \sum_{j=0}^{q} iB_{ij} \left(\frac{x}{L} \right)^{i-1} \left(\frac{y}{H} \right)^j \right) \end{cases} \tag{20}$$

Substituting the above expressions of the virtual strain components in Eq. (5) provides four equations where the A_{ij}'s and the B_{ij}'s are the unknowns. These four equations are not reported here for the sake of legibility.

Eventually, a linear system of $4+q$ equations where the A_{ij}'s and the B_{ij}'s are the unknowns is obtained

$$\mathbf{DY} = \mathbf{E} \tag{21}$$

where $\mathbf{D}$ is a rectangular matrix with as many columns as unknown coefficients A_{ij}'s and B_{ij}'s. Its number of rows depends on the number of monomials used in the virtual displacement field, $\mathbf{E}$ is a vector where components are equal to 0 or 1 and $\mathbf{Y}$ is a vector whose components are the unknowns

$$\mathbf{Y}: \begin{bmatrix} A_{00} \\ \cdot \\ A_{01} \\ \cdot \\ A_{mn} \\ B_{00} \\ B_{01} \\ \cdot \\ B_{pq} \end{bmatrix} \tag{22}$$

Let us now examine how to solve in practice such a linear system.

3.7. Strategy for solving the final linear system

The first step for solving the final linear system is to fix a value for m, n, p, q. In our example, it is suggested to use $m = 1$, $n = 3$, $p = 2$, $q = 3$. This choice is justified a posteriori, with the number of rows and columns in matrix $\mathbf{D}$. In this case $(m+1)\times(n+1)+(p+1)\times(q+1) = 2\times 4+3\times 4 = 20$ unknowns whereas $4+q = 4+3 = 7$ equations are available. This result illustrates the fact that an infinity of solutions will be found a priori. It allows in practice the determination of many values of the unknown stiffnesses. At this stage, the determination of the remaining coefficients A_{ij} and B_{ij} is carried out as follows.

N different possible square matrices may be extracted from $\mathbf{D}$, with $N = 20!/7!(20-7)! = 20!/7!13! = 77\,520$. Let $\mathbf{G}'$ be the 7×7 square matrix and $\mathbf{G}''$ the matrix built up with the $20-7 = 13$ remaining columns. The dimension of $\mathbf{G}''$ is 7×13. In each of the N cases, the determinant $\det(\mathbf{G}')$ is computed. Since the components of $\mathbf{D}$ are normalized, the value of this determinant provides an information concerning the degree of independence of the equations. Another value could be used for selecting the square matrices: their condition number, but this approach has not been used here for numerical reasons which are not detailed here. Eventually, only the cases in which the determinant is greater than a fixed value $\det_{\min}$ are kept and each of them provides a value of the identified stiffness. In these cases, the unknowns are calculated as follows. The 13 columns of $\mathbf{G}''$ correspond to some components of $\mathbf{Y}$ which values can be fixed randomly a priori between two bounds denoted hereafter $\pm$mag. Let $\mathbf{Y}''$ be the vector built up with these 13 random values and $\mathbf{Y}'$ the vector built up with the seven remaining unknowns. The new linear system may be written as

$$\mathbf{G}'\mathbf{Y}' = \mathbf{E} - \mathbf{G}''\mathbf{Y}'' \tag{23}$$

and the seven unknowns in $\mathbf{Y}'$ are finally determined by inversion of $\mathbf{G}'$, since only the cases where $\det \mathbf{G}' \neq 0$ are considered

$$\mathbf{Y}' = \mathbf{G}'-1(\mathbf{E} - \mathbf{G}''\mathbf{Y}''), \quad \det \mathbf{G}' \neq 0 \tag{24}$$

Eventually, the vectors $\mathbf{Y}'$ and $\mathbf{Y}''$ directly give the unknown coefficients A_{ij} and B_{ij}. All these coefficients are collected and the corresponding identified stiffnesses are sorted, as will be shown below. As a conclusion, the procedure is summed up in the flow-chart in Fig. 3.

The program has been developed in practice with the Matlab package. The above procedure carried out with a typical example like those presented below requires about 3mn with a Pentium III 866 MHz/512 MB RAM.

3.8. Simple expression of the unknown parameters

It must be emphasized that with such virtual fields in Eq. (17), the virtual work of the external loading, which is the right-hand side in Eq. (3), may be written very simply

$$\int_{S_f} T_i \hat{u}_i^* \, \mathrm{d}S = (B_{00} + B_{10} + B_{20}) \times F \tag{25}$$

Let us consider for instance the particular case where Q_{xx} is to be determined. We can easily deduce from Eq. (17) a very simple expression for the unknown Q_{xx}

$$Q_{xx} = (B_{00} + B_{10} + B_{20}) \times F \tag{26}$$

It is relevant to note that in the present case, the mechanical parameter to be determined only depends on three coefficients: B_{00}, B_{10} and B_{20}, which are three of the 20 coefficients that characterize the special virtual field for Q_{xx}.

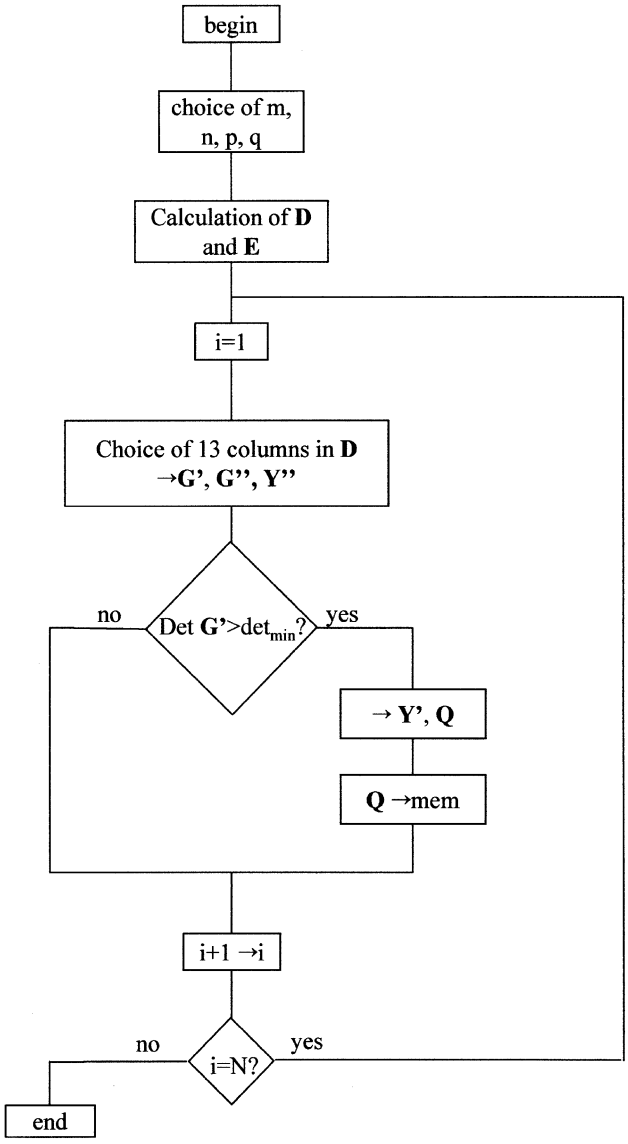

Fig. 3. Flow-chart of the procedure for determining automatically the virtual fields.

4. Numerical simulations

4.1. Finite element model

Since this paper only focuses on the identification method and on the automatic determination of the virtual fields, no experimental data are presently processed. The strain fields are obtained with finite element simulations. The materials tested are reported in Table 1. The fourth one exhibits non-linear behavior. In the following sections, the strain fields corresponding to materials 1 and 4 are obtained with the CASTEM 2000 package whereas those corresponding to materials 2 and 3 are obtained with the ANSYS package.

Table 1
Mechanical parameters of different materials

Material #	Q_{xx} (GPa)	Q_{yy} (GPa)	Q_{xy} (GPa)	Q_{ss} (GPa)	$Q_{ss}^{(3)}$ (GPa)
1	25.94	10.37	3.11	4.00	–
2	180.36	10.02	3.01	5.00	–
3	10.02	180.36	3.01	5.00	–
4	25.94	10.37	3.11	4.00	−4420

The model of the surface S' exhibits 7200 triangular elements in the first case and 2400 quadrilateral linear elements in the second case. The boundary conditions are such that the contact between the grips and the specimen is compressive only (Ho et al., 1994).

4.2. Tuning the program

The strain components as well as the coordinates at the center of the elements of the finite element model are first collected over S'. They are considered as simulated input data for the identification procedure. It must be emphasized that the number of points presently considered for the calculations is much lower than the number of points that would be processed in practice. The present mesh of S has 2400 elements whereas a CCD grid of 1000×1000 pixels would provide up to 10^6 experimental values. It is clear that this extra information would improve the quality of the results.

The first step is to compute all the integrals involved in matrix $\mathbf{D}$. The identification procedure is then carried out according to the flow-chart in Fig. 3. One value must be determined: $\det_{\min}$, the threshold value over which the inversion of $\mathbf{G}'$ is done. In order to fix $\det_{\min}$, the program is run once. The N values of the determinants $\det \mathbf{G}'$ are collected. As explained above, $\det \mathbf{G}'$ is an indicator of the degree of independence of the rows and columns in $\mathbf{G}'$, and therefore an indicator on the sensitivity of the identified value to noisy data. The value of $\det_{\min}$ is chosen in such a way that some tens of the highest values of $\det \mathbf{G}'$ are considered for the determination of the unknowns. The N values of the determinant are reported in Fig. 4. It is

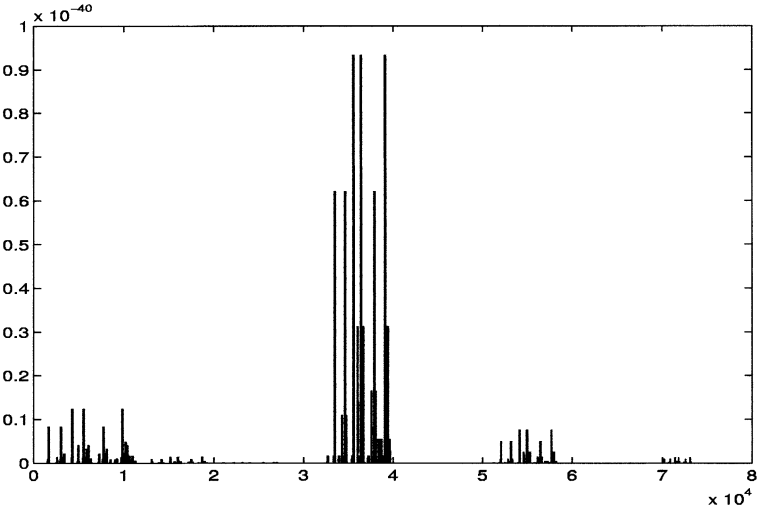

Fig. 4. $N = 77\,440$ values of the determinant $\det \mathbf{E}'$.

worth noting that det $\mathbf{G}'$ is zero or very small in many cases. They correspond to the cases where two columns or two rows at least are proportional or quasi-proportional, or to the cases where one line is zero. This last case often occurs because of Eq. (19). In the present case, three such equations are obtained. Each of them only involves three unknowns B_{ij}. For instance, the first equation may be written as

$$B_{10} + B_{11} + B_{12} = 0 \tag{27}$$

It corresponds to the fifth line in matrix $\mathbf{D}$. If one of the columns in $\mathbf{D}$ corresponding to the unknowns B_{10}, B_{11} and B_{12} is not in $\mathbf{G}'$, a line of zeros appears in $\mathbf{G}'$ and det $\mathbf{G}' = 0$. This case often occurs since the fifth line in $\mathbf{D}$ has at most three non-zero terms and at least $20 - 3 = 17$ zeros.

The value of $\det_{\min}$ is chosen just below the maximum value of the determinant: 8×10^{-41} in the present case. This choice could be done automatically, for instance by choosing 10% of the maximum value of the determinant. In practice, only 282 values are presently collected from the $N = 77\,440$ combinations of columns, that is 2.47%. It means that 282 values of Q_{xx}, Q_{yy}, Q_{xy} and Q_{ss} are available. To obtain either Q_{xx}, Q_{yy}, Q_{xy} or Q_{ss}, only the location of the "1" in the first four components in vector $\mathbf{E}$ in Eq. (21) is changed, according to Eq. (5). For instance, for finding Q_{xx}: $E_1 = 1$, $E_2 = E_3 = E_4 = 0$, for finding Q_{yy}: $E_2 = 1$, $E_1 = E_3 = E_4 = 0$ etc...

4.3. Examples of special virtual fields

The program has been run with the $\det_{\min} = 8 \times 10^{-41}$ and mag $= 0$. Each of these 282 cases provides a value for Q_{xx}, Q_{yy}, Q_{xy} and Q_{ss}. The mean, minimum and maximum values of each of these parameters are reported in Table 2. As can be observed, the difference between both the minimum and the maximum values is very small, showing a very good coherence in the results.

The 50 first fields obtained for each of these stiffnesses are plotted in Fig. 5. Several points are worth noting.

- Each unknown stiffness Q_{xx}, Q_{yy}, Q_{xy} and Q_{ss} is equal to the external virtual work obtained with the four special virtual fields in Fig. 5(a)–(d) respectively. Each unknown is therefore directly proportional to the virtual displacement of the right-hand side grip since the loading is applied on this side of the specimen. Indeed, it can be observed that the vertical virtual displacement of the right-hand grip is the greatest in case (a), then in case (b), then in case (d) and finally in case (c), according to the value of the reference stiffnesses of material 1 (Table 1).
- For each stiffness component, all the special virtual fields provide about the same value of the virtual displacement of the right-hand grip. This clearly illustrates the very low scatter of the identified values.
- For each stiffness component, the special virtual fields are very similar and correspond to some small variations about an "average" field.
- It clearly appears that the global distortion of the fields depends on the stiffness. "Distortion" means here that the virtual vertical displacement of the right-hand grip is small whereas the vertical or horizontal virtual displacement of some points in the central part of the specimen is very large. It has been observed that this feature is directly related to the influence of each parameter on the actual field. The more

Table 2
Identified stiffnesses without noise, material 1

Material	Q_{xx} (GPa)	Q_{yy} (GPa)	Q_{xy} (GPa)	Q_{ss} (GPa)
Reference	25.94	10.37	3.11	4.00
Identified min	25.96	10.14	3.03	4.00
Identified mean	25.97	10.24	3.10	4.00
Identified max	26.01	10.27	3.11	4.00

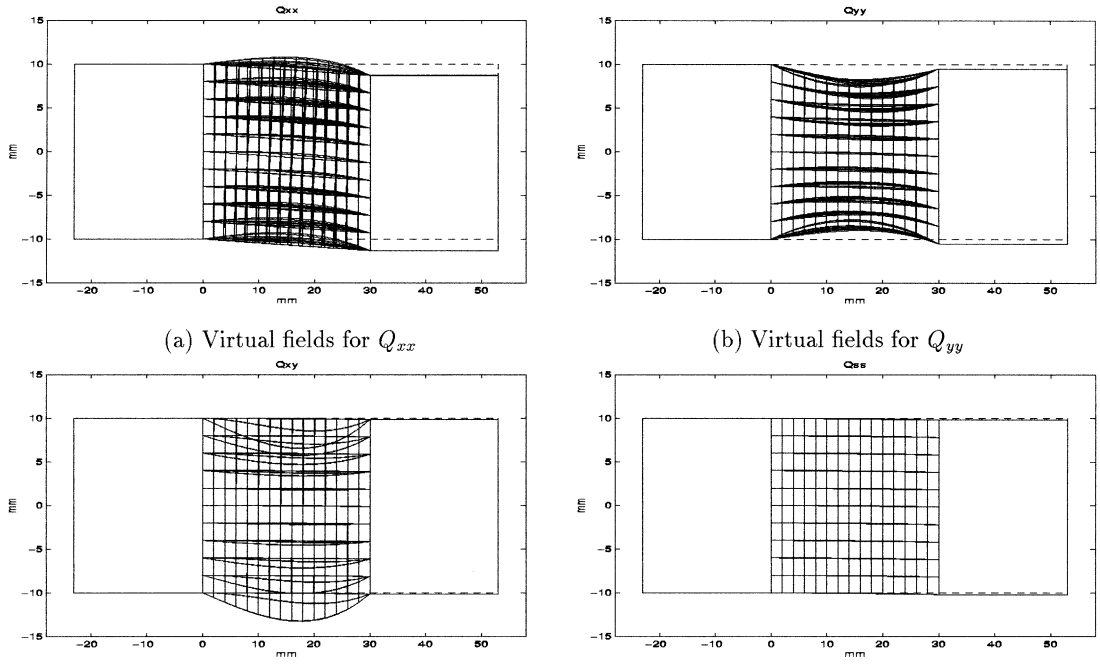

(a) Virtual fields for Q_{xx} (b) Virtual fields for Q_{yy}

(c) Virtual fields for Q_{xy} (d) Virtual fields for Q_{ss}

Fig. 5. Special virtual fields for each of the four stiffnesses, material 1.

influential the parameter in the actual field is, the less the distortion is. It will be shown below that this feature is also directly related to the stability of the results.

4.4. Stability of the results

A very important point in this type of inverse problem is the sensitivity to noisy data. Two types of errors were considered in this work. First, a white noise was added to the strain values provided by the finite element program. It was observed that the identified stiffnesses were only very slightly affected by this noise. The reason is certainly the "average effect" that occurs when the integrals are computed. These results are therefore not discussed here.

Another type of error is more relevant: the influence of a shift in the coordinate system. This type of error is similar to the error which occurs in practice since the actual field is expected to be captured by a CCD camera. The data are therefore processed in the basis of the model that not necessarily matches the basis of the specimen since a shift may occur between these two bases. The influence of such an error on the identified parameters can be assessed by adding a constant value to the coordinates of the points where the strain components are provided by the finite element program. In the present study, this constant is equal to a percentage p of the length L and the height H. Four cases have been studied: $p = 1\%$, 2%, 3%, 4%. In each case, a constant value $p \times L$ is added to the x-coordinate of the points in the calculation of the integrals that are used to build up matrix $\mathbf{D}$. In the same way, a constant value $p \times H$ is added to the y-coordinate of the points. The same procedure as above was carried out and the identified parameters were collected. It was observed that the scatter of the results increased with p, i.e. the difference between the maximum and the minimum of each stiffness component increased. The distribution about the actual value

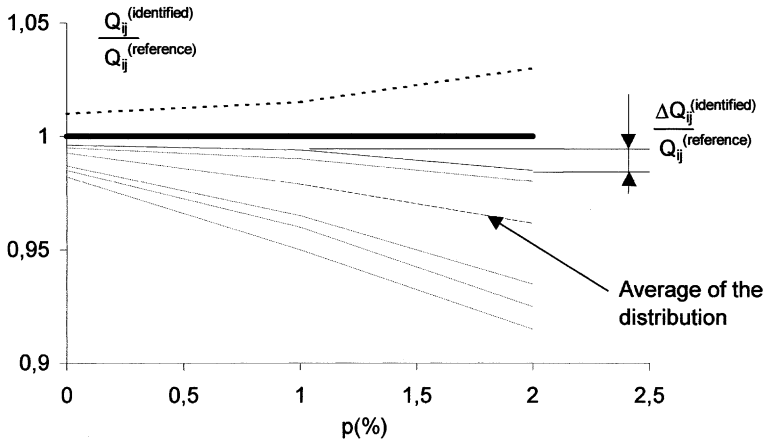

Fig. 6. Typical influence of a shift on an identified stiffness.

is not regular, as schematically illustrated in Fig. 6. At this stage, the problem is to find the "optimal" value among all identified values. Two methods can be considered for that:

- *Method 1:* The first method is to compute the average of the distribution. The results obtained in a particular case, $p = 4\%$, are reported in Table 3, row 2.
- *Method 2:* It was observed that the distribution about each of the reference values was not uniform (see Fig. 6). Let us consider that the optimized stiffness is the value provided by a special virtual field which is the less sensitive to a shift. To find it, we compute first the variation of each stiffness ΔQ_{ij} when the shift p increases by 1%

$$\Delta Q_{ij} = Q_{ij}(p) - Q_{ij}(p + 1\%) \tag{28}$$

The "score" $\mathrm{Sc}(\hat{\mathbf{u}}^*)$ of each special field $\hat{\mathbf{u}}^*$ is then assessed by the following quantity

$$\mathrm{Sc} = \sqrt{\Delta Q_{xx}^2 + \Delta Q_{yy}^2 + \Delta Q_{xy}^2 + \Delta Q_{ss}^2} \tag{29}$$

The optimized virtual field is the special virtual field that exhibits the lowest score. It corresponds to the virtual field that is the less sensitive to a shift. In practice, the score of each of the 282 special virtual fields is computed and the optimized field is detected with the lowest score Sc. Six distributions only have been schematically reported in Fig. 6 for the sake of legibility. They are plotted vs. the shift p. It clearly appears that the identified values are not uniformly distributed about the actual value. For each stiffness, the average is therefore lower than the value that exhibits the lowest variation ΔQ_{ij}.

Table 3
Identified stiffnesses with a shift $p = 4\%$, material 1

Material	Q_{xx} (GPa)	Q_{yy} (GPa)	Q_{xy} (GPa)	Q_{ss} (GPa)
Reference	25.94	10.37	3.11	4.00
Method 1	22.13	13.31	2.65	3.74
	−14.3%	28.3%	−14.8%	−1.5%
Method 2	25.71	11.38	3.08	4.00
	−0.5%	9.7%	−1%	0%

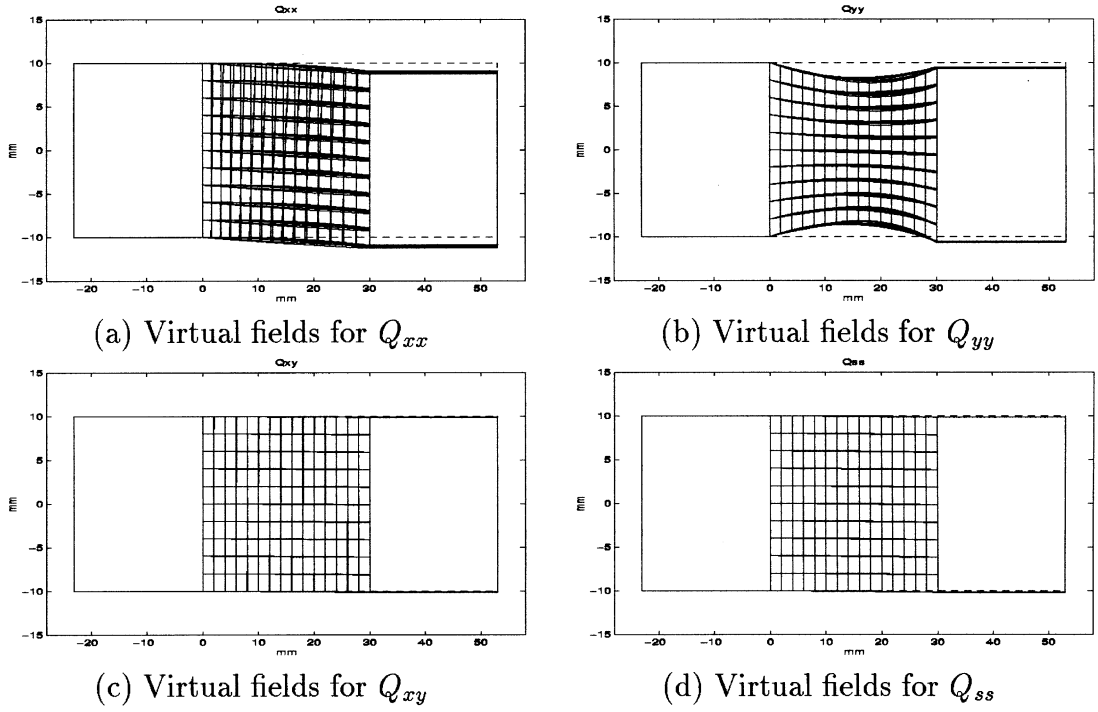

Fig. 7. Special virtual fields for each of the four stiffnesses, material 1, $p = 4\%$.

The results obtained with this second method are also reported in Table 3, row 3. They clearly illustrate the efficiency of this second method. The 50 first virtual fields found in the case $p = 4\%$ are plotted in Fig. 7 to illustrate the scatter of the special virtual fields. Bearing in mind that the identified stiffnesses are equal in each case to the external virtual work, the distribution of these identified stiffnesses is directly related to the distribution of the virtual vertical displacements of the right-hand side grip. The graphical results in Fig. 7 are in good agreement with the result in Table 3 and the scatter of each of the four stiffnesses clearly appears through the scatter of the vertical virtual displacement of the right-hand side grip.

Finally, the expression of the optimized virtual fields $\hat{\mathbf{u}}^{*(1)}$, $\hat{\mathbf{u}}^{*(2)}$, $\hat{\mathbf{u}}^{*(3)}$ and $\hat{\mathbf{u}}^{*(4)}$ is given below. They directly provide the optimized values of the stiffnesses in Table 3, row 3.

$$\begin{cases} \hat{u}_x^{*(1)} = \frac{x(x-L)}{L^2}\left(5.91 - 6.56\frac{y}{L}\right) \times 10^5 \\ \hat{u}_y^{*(1)} = -1.63 \times \frac{x}{L} \times 10^5 \\ \hat{u}_x^{*(2)} = \frac{x(x-L)}{L^2}\left(-0.2387 - 0.0095\frac{y}{H}\right) \times 10^6 \\ \hat{u}_y^{*(2)} = \frac{x}{L}\left(-0.0719 - 1.6781\frac{y}{H}\left(1 - \frac{x}{L}\right)\right) \times 10^6 \\ \hat{u}_x^{*(3)} = \frac{x(x-L)}{L^2}\left(-1.98 - 0.0785\frac{y}{H}\right) \times 10^6 \\ \hat{u}_y^{*(3)} = 0.0194 \times \frac{x}{L} \times 10^6 \\ \hat{u}_x^{*(4)} = 0 \\ \hat{u}_y^{*(4)} = -2.526 \times \frac{x}{L} \times 10^4 \end{cases} \tag{30}$$

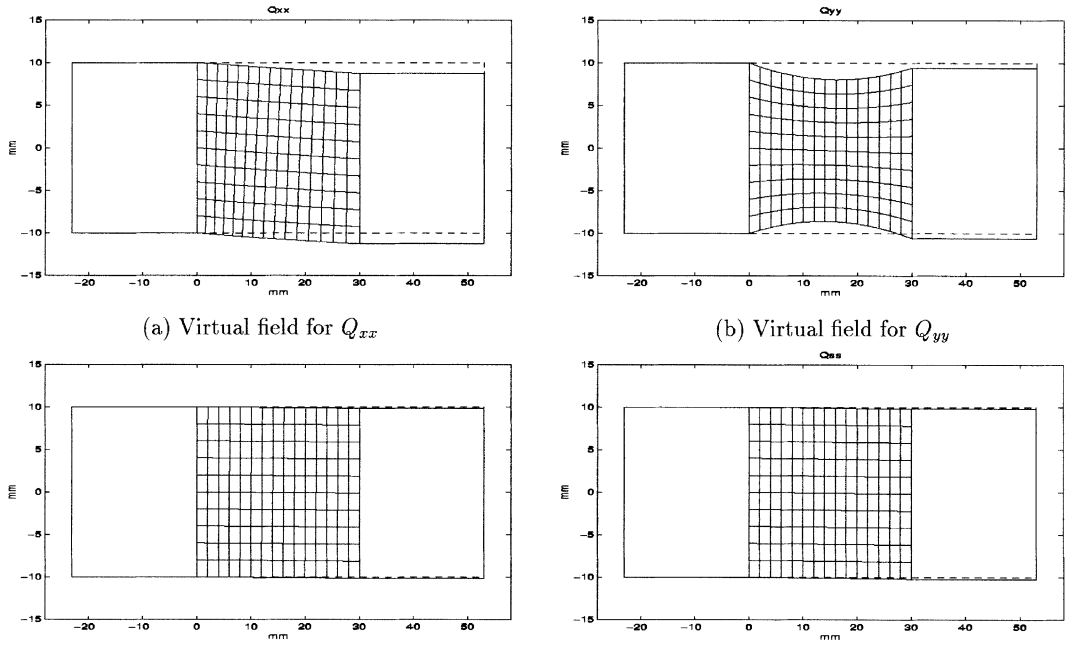

(a) Virtual field for Q_{xx}

(b) Virtual field for Q_{yy}

(c) Virtual field for Q_{xy}

(d) Virtual field for Q_{ss}

Fig. 8. Optimized virtual fields, material 1, $p = 4\%$.

As can be seen, only a basis of five monomials among the 20 in Eq. (17) are necessary to build the optimized virtual fields: 1 and y/H for u_x^*; 1, y/H and xy/LH for $\hat{u}_y^*$. The five corresponding coefficients A_{00}, A_{01}, B_{00}, B_{01} and B_{11} are determined for each special virtual field $\hat{\boldsymbol{u}}^{*(1)}$, $\hat{\boldsymbol{u}}^{*(2)}$, $\hat{\boldsymbol{u}}^{*(3)}$, and $\hat{\boldsymbol{u}}^{*(4)}$. It should be noted that the second one is the more complicated one and corresponds to the stiffness component which is the most sensitive to noisy data. It can be observed that the fourth virtual field is rather simple, since it leads to a constant virtual shear strain. It corresponds to the stiffness component which is the less sensitive to noisy data. Such a simple virtual field was guessed in a previous work to obtain directly Q_{ss} (Pierron and Grédiac, 2000; Grédiac et al., 2001). On the other hand, the three other fields cannot be easily guessed a priori. The link between the number of terms in the virtual field, the power of the monomials and the stability and the accuracy of the results can be clearly observed. This feature was already detected in the early developments of the virtual fields method (Grédiac and Vautrin, 1990). Finally, the optimized virtual fields found with method 2 are plotted in Fig. 8.

4.5. Influence of the magnitude mag of the coefficients fixed a priori

The magnitude mag of the coefficients fixed randomly a priori was set to zero in the above simulations. The effect of a non-zero magnitude is illustrated in Fig. 9, where the 25 first virtual fields obtained with a shift $p = 4\%$ and a magnitude $\text{mag} = 2 \times 10^6$ instead of 0 are plotted. As can be clearly seen, the scatter is much higher than in Fig. 7, because of additional terms in the expression of the special virtual fields. It has been observed that these new virtual fields do not provide any additional information, but rather an additional noise. This is directly related to the observation that the stability and the accuracy of the identification are related to the simplicity of the virtual fields, as observed above. For this reason, the parameter mag is always set to zero in the following.

4.6. Influence of the anisotropy

4.6.1. Introduction

Other materials were tested to examine the influence of the anisotropy. Their mechanical properties are reported in Table 1. These materials correspond to a unidirectional graphite/epoxy composite (i.e. a very anisotropic material) (Tsai and Hahn, 1980) which fibers are oriented either at 0° or at 90°.

4.6.2. Fibers at 0°

The fibers are first aligned with the x-axis of the specimen. Method 2 above has been applied and the results are reported in Table 4. As can be seen, the influence of a shift on the stiffnesses is very small. The most sensitive coefficient is Q_{yy}. The optimized virtual fields corresponding to the four stiffnesses are plotted in Fig. 10. The difference between the orders of magnitude between the stiffnesses is clearly visible, since the virtual displacement of the right-hand side grip is much more important in case (a), which is the case of the virtual field that directly provides Q_{xx}. For this material, the four optimized virtual fields may be written as

$$\begin{cases} \hat{u}_x^{*(1)} = \frac{x(x-L)}{L^2}\left(0.434\frac{x}{L} - 1.003\frac{y}{L}\right) \times 10^6 \\ \hat{u}_y^{*(1)} = -0.2484 \times \frac{x}{L} \times 10^5 \\ \hat{u}_x^{*(2)} = \frac{x(x-L)}{L^2}\left(-0.0028\frac{y}{H} - 0.0201\frac{x}{H}\right) \times 10^5 \\ \hat{u}_y^{*(2)} = \frac{x}{L}\left(-0.1506 - 2.917\frac{y}{H}\left(1-\frac{x}{L}\right)\right) \times 10^6 \\ \hat{u}_x^{*(3)} = \frac{x(x-L)}{L^2}\left(-1.2072\frac{x}{L} - 0.1672\frac{y}{H}\right) \times 10^5 \\ \hat{u}_y^{*(3)} = -0.0414 \times \frac{x}{L} \times 10^6 \\ \hat{u}_x^{*(4)} = 0 \\ \hat{u}_y^{(4)} = -6.526 \times \frac{x}{L} \times 10^3 \end{cases} \tag{31}$$

The polynomials used for this material are similar to the polynomials used for the previous material: only 1 has been changed into x/L in the expression of $\hat{u}_x^*$. As an example, both the actual ϵ_x and the virtual $\hat{\epsilon}_x^{*(1)}$ strain fields are plotted in Fig. 11(a) and (b) respectively. As can be seen, both of them are very different. The product $\hat{\epsilon}_x^{*(1)} \times \epsilon_x$ is plotted in Fig. 11(c). It clearly appears that the strain field is mainly involved near the corners of the central part of the specimen. This is due to the fact that the actual strain component is important in the vicinity of the corners because of the contact with the supports. To avoid this, other calculations should be performed with a reduced part of the central zone, far away from the supports. Theoretically, the special strain field is such that $\int_S \hat{\epsilon}_x^{*(1)}\epsilon_x \, dS = 1$ (see the first set of equalities in Eq. (5)). It can be verified that we obtain in the present case 0.9922 instead of 1 because of numerical approximations. In the same way, it has been checked that the average of the virtual strain $(1/S)\int_S \epsilon_x^{*(1)} \, dS$ is very close to zero since the virtual horizontal displacement at $x = 0$ and $x = L$ are zero.

4.6.3. Fibers at 90°: influence of the actual field

The fibers are then considered to lie in the y-axis. The results are reported in Table 5, row $L = 30$ mm. As can be seen, the identified stiffnesses are no more realistic beyond $p = 2\%$. The probable reason is the very low influence of the stiffness along the fibers in such a configuration. A close inspection of the actual strain fields shows that the magnitude of the transverse normal strain ϵ_y is very low compared to the two other strain components. Another simulation has been performed with $L = 10$ mm: the distance between the grips has been reduced, as allowed in practice by the setup described in Pierron and Vautrin (1997). It has been observed that the actual strain components are much more balanced. The identified stiffnesses are reported in Table 5, row $L = 10$ mm. As can be seen, the identified values are more stable than in the above case. In

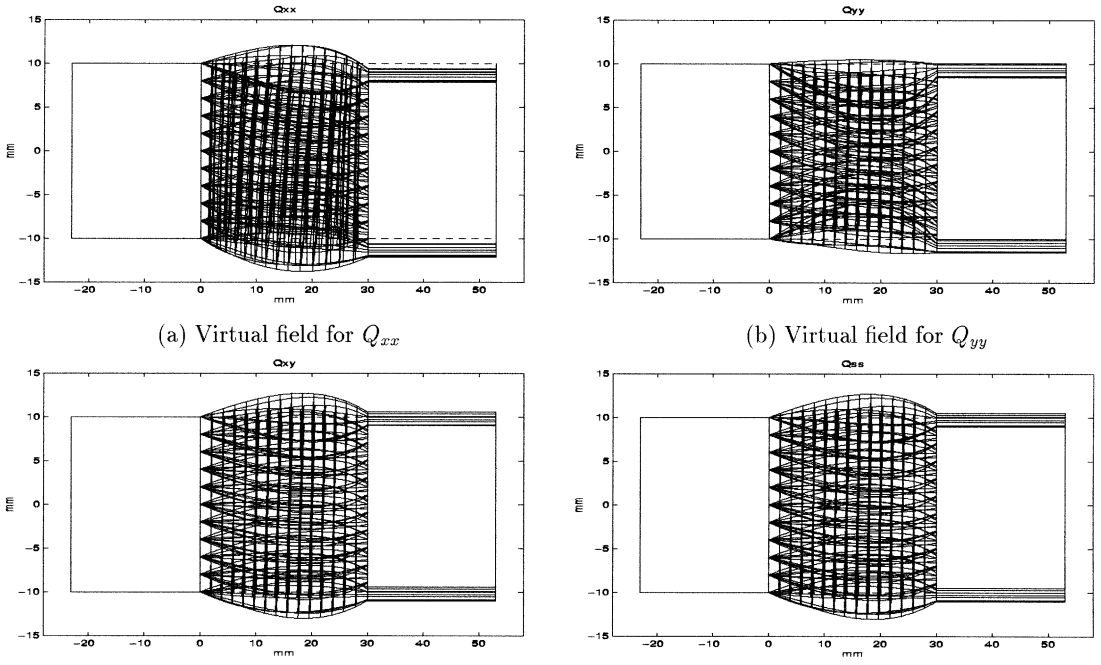

(a) Virtual field for Q_{xx} (b) Virtual field for Q_{yy}

(c) Virtual field for Q_{xy} (d) Virtual field for Q_{ss}

Fig. 9. Special virtual fields, material 1, $p = 4\%$, mag $= 2 \times 10^6$.

Table 4
Identified stiffnesses, material 2

p (%)	Q_{xx} (GPa)	Q_{yy} (GPa)	Q_{xy} (GPa)	Q_{ss} (GPa)
Reference	180.36	10.02	3.01	5.00
0	181.19	10.02	3.02	5.00
	−0.09%	0%	0.03%	0%
1	181.08	10.07	3.02	5.00
	−0.15%	0.5%	0.03%	0%
2	180.70	10.23	3.00	5.00
	−0.36%	2.1%	−0.03%	0%
3	180.21	10.50	3.00	5.00
	−0.63%	4.8%	−0.03%	0%
4	179.45	10.88	2.99	5.00
	−1.05%	8.58%	−0.07%	0%

conclusion, it is clear that the actual stress/strain fields directly influence the accuracy and the stability of the results: mechanical configurations with a balanced influence of each mechanical parameters are probably the most suitable for such an identification procedure.

4.7. Identification of a coefficient governing a non-linear response

The above example deals with elastic linear responses of composite materials. However, such materials often exhibit a *non-linear* response, mainly in shear. The idea here is to examine the capability of the present

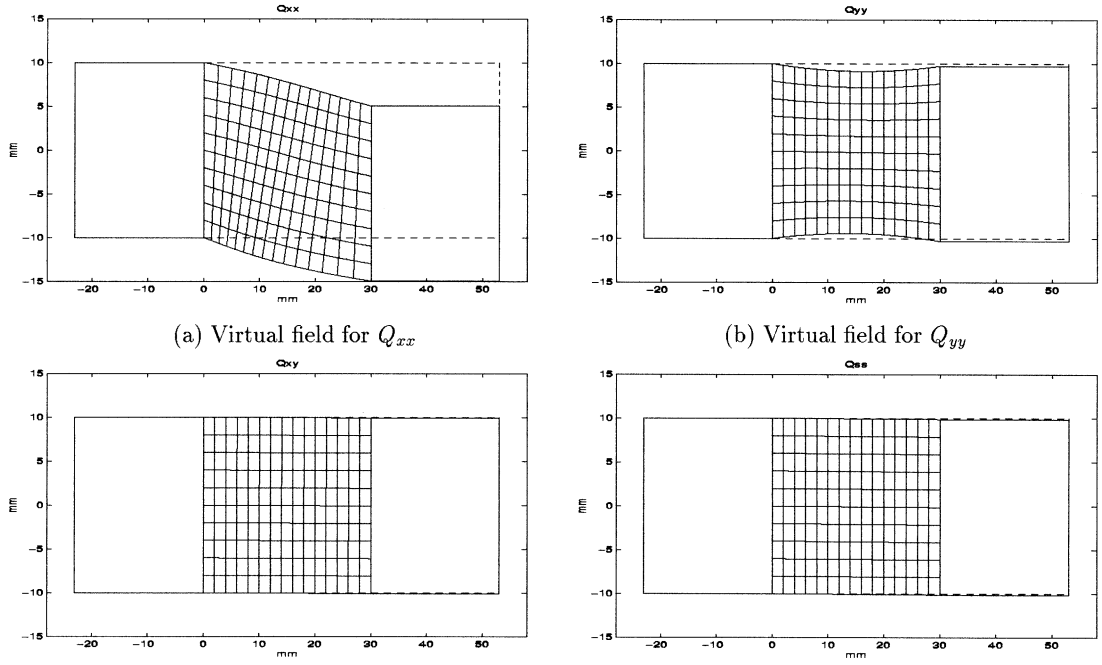

(a) Virtual field for Q_{xx} (b) Virtual field for Q_{yy}

(c) Virtual field for Q_{xy} (d) Virtual field for Q_{ss}

Fig. 10. Optimized virtual fields, material 2, $p = 4\%$.

approach to identify a parameter governing a non-linear shear response in the case of material 1. The shear stress/strain response is presently written as

$$\sigma_s = Q_{ss}\epsilon_s + Q_{ss}^{(3)}\epsilon_s^3 \tag{32}$$

Such a polynomial law was found to fit correctly the shear response of a glass/epoxy composite studied in Refs. Cerisier (1997) and Swansson et al. (1985). The mechanical characteristics of this material are reported in Table 1 (material 4). The shear stress/strain curve is plotted in Fig. 12 and the goal is here to retrieve $Q_{ss}^{(3)}$ that govern the softening of the shear response as well as the four other parameters. It should be emphasized that the *whole* curve in Fig. 12 is present in the global response of the specimen, since the shear stress is zero at the free edge and maximum at the center of the specimen if the load level is well chosen. One can therefore expect to identify correctly the parameter that governs the softening of the curve. As a first attempt, the virtual fields method was applied with a set of virtual fields found intuitively (Grédiac et al., 2001). It was somewhat difficult to find five independent virtual fields, and one had to consider several actual fields to obtain acceptable results in terms of stability. The above method is presently applied to find $Q_{ss}^{(3)}$ from data supplied by the finite element simulation. In this case, the principle of virtual field may be written as

$$I_{xx}Q_{xx} + I_{yy}Q_{yy} + I_{xy}Q_{xy} + I_{ss}Q_{ss} + I_{ss}^{(3)}Q_{ss}^{(3)} = \int_{\partial S_1} T_i u_i^* \tag{33}$$

with

$$I_{ss}^{(3)} = \int_S \epsilon_s^3 \epsilon_s^* \, \mathrm{d}S \tag{34}$$

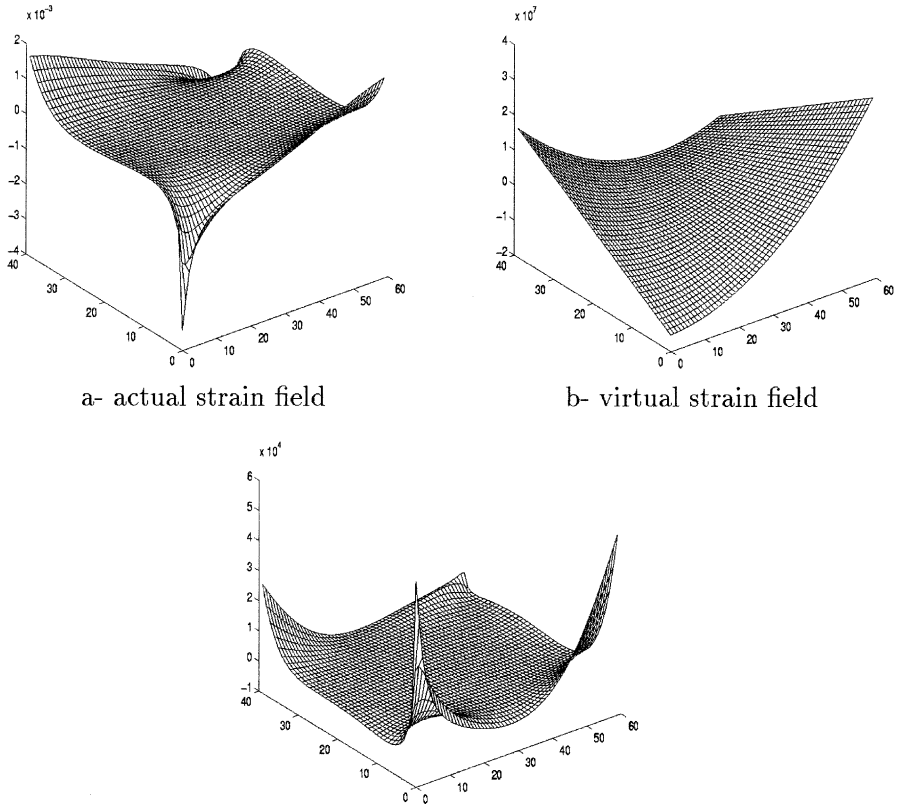

a- actual strain field

b- virtual strain field

c- product between the actual and the virtual strain fields

Fig. 11. Actual strain field $\hat{\epsilon}_x^{*(1)}$ and virtual strain field ϵ_x, material 2, $p = 4\%$.

As explained in Ref. Grédiac et al. (2001), the central part of the specimen is presently about 80% of the central part processed in the case of elasticity for numerical reason. Indeed, the cubic law is followed by a linear response (see Fig. 12). Since some local high values of the stress occur near the grip, they correspond to this linear response. Strain data collected in this part of the specimen are therefore not suited to the identification of the parameter which governs the cubic part of the law and are consequently removed from the processed data.

If one wishes to find a virtual field $\hat{\mathbf{u}}^{*(5)}$ which directly provides $Q_{ss}^{(3)}$ by filtering the actual field, condition 2 in Section 3.1 provides a fifth set of equations between the coefficients of the polynomials, that is

$$\mathbf{u}^{*(5)} : I_{ss}^{(3)} = 1, \quad I_{xx} = I_{yy} = I_{xy} = I_{ss} = 0 \tag{35}$$

Consequently, matrix $\mathbf{D}$ has now eight lines instead of seven in the above sections, and the dimension of the final square matrix $\mathbf{G}'$ is eight instead of seven. The number of column combinations is here $N = 20!/8!(20-8)! = 20!/8!12! = 125\,970$. The values of the parameters identified with method 2 are reported in Table 6 vs. the shift p. As a general remark, the mechanical parameters are obtained with a higher sensitivity to noisy data than in the case of linear elasticity. The stability however remains acceptable. Note finally that $Q_{ss}^{(3)}$, which governs the non-linear response, is always lower than the reference value. A possible reason is the fact that the number of iterations in the finite element calculations was not sufficient to model

Table 5
Identified stiffnesses, material 3

p (%)	L (mm)	Q_{xx} (GPa)	Q_{yy} (GPa)	Q_{xy} (GPa)	Q_{ss} (GPa)
Reference	–	10.02	180.36	3.01	5.00
0	30	10.06	172.64	2.85	5.00
		0.4%	−4.3%	−5.3%	0%
	10	10.10	172.30	3.04	5.00
		0.9%	−4.5%	1.0%	0%
1	30	9.76	170.74	3.32	4.85
		−2.6%	−5.3%	10.3%	−3.0%
	10	9.80	168.85	2.95	5.00
		−2.1%	−6.4%	−2%	−2.8%
2	30	9.46	173.37	<0	4.70
		−5.6%	−3.9%	–	−5.8%
	10	9.50	168.37	2.85	5.00
		−5.1%	−6.6%	−5.3%	−5.8%
3	30	9.44	<0	<0	4.70
		−5.8%	–	–	−5.8%
	10	9.20	170.79	2.76	4.58
		−8.1%	−5.3%	−8.3%	−8.4%

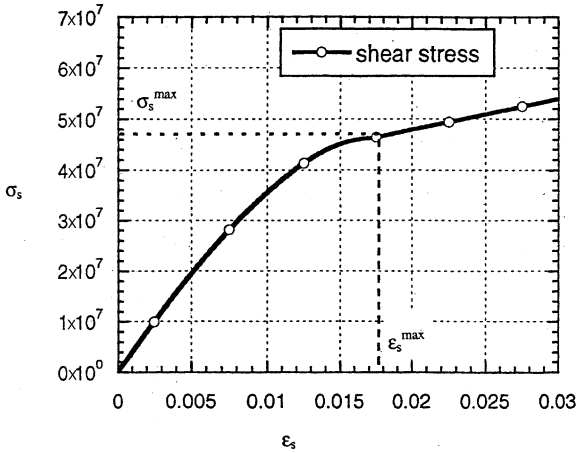

Fig. 12. Cubic law (Grédiac et al., 2001).

Table 6
Identified parameters, material 4

p (%)	Q_{xx} (GPa)	Q_{yy} (GPa)	Q_{xy} (GPa)	Q_{ss} (GPa)	Abs($Q_{ss}^{(3)}$) (GPa)
Reference	25.94	10.37	3.11	4.00	4420
1	26.90	9.58	2.24	4.02	4192
	3.70%	−7.6%	−28.%	0.5%	−5.2%
2	27.25	9.78	3.91	4.01	4116
	5.1%	−5.7%	25.7%	0.3%	−6.5%
3	27.23	9.74	3.75	4.01	4155
	5.0%	−6.1%	20.58%	0.3%	−6.0%
4	27.13	9.72	3.47	4.02	4169
	4.6%	−6.3%	11.6%	0.5%	−5.7%

correctly the non-linear response of the material. In fact, both the present identification method and the finite element program that provides the simulated experimental data are tested simultaneously.

The corresponding optimized virtual fields obtained at $p = 4\%$ are plotted in Fig. 13. For the sake of legibility, $Q_{ss}^{(3)}$ has been divided by -1000 to obtain virtual displacements comparable to other ones. The four first virtual fields in Fig. 13 are very similar to those obtained in the above section. The fifth one directly provides $Q_{ss}^{(3)}$. It is worth noting that this virtual field induces a virtual warping of the sections which vanishes near the left and right-hand side boundaries.

Contrary to the preceding case, it was presently observed that two types of special virtual fields could be distinguished, as can be seen in Fig. 13(f) in the case of $Q_{ss}^{(3)}$. On close inspection, it was observed that the first type corresponds to the cases where two parameters among B_{00}, B_{10} and B_{20} are zero (these three parameters provide the unknown parameters, see Eq. (26) in the case of Q_{xx}). The second type corresponds to the cases where one parameter only among B_{00}, B_{10} and B_{20} is zero. In the former case, the unknown

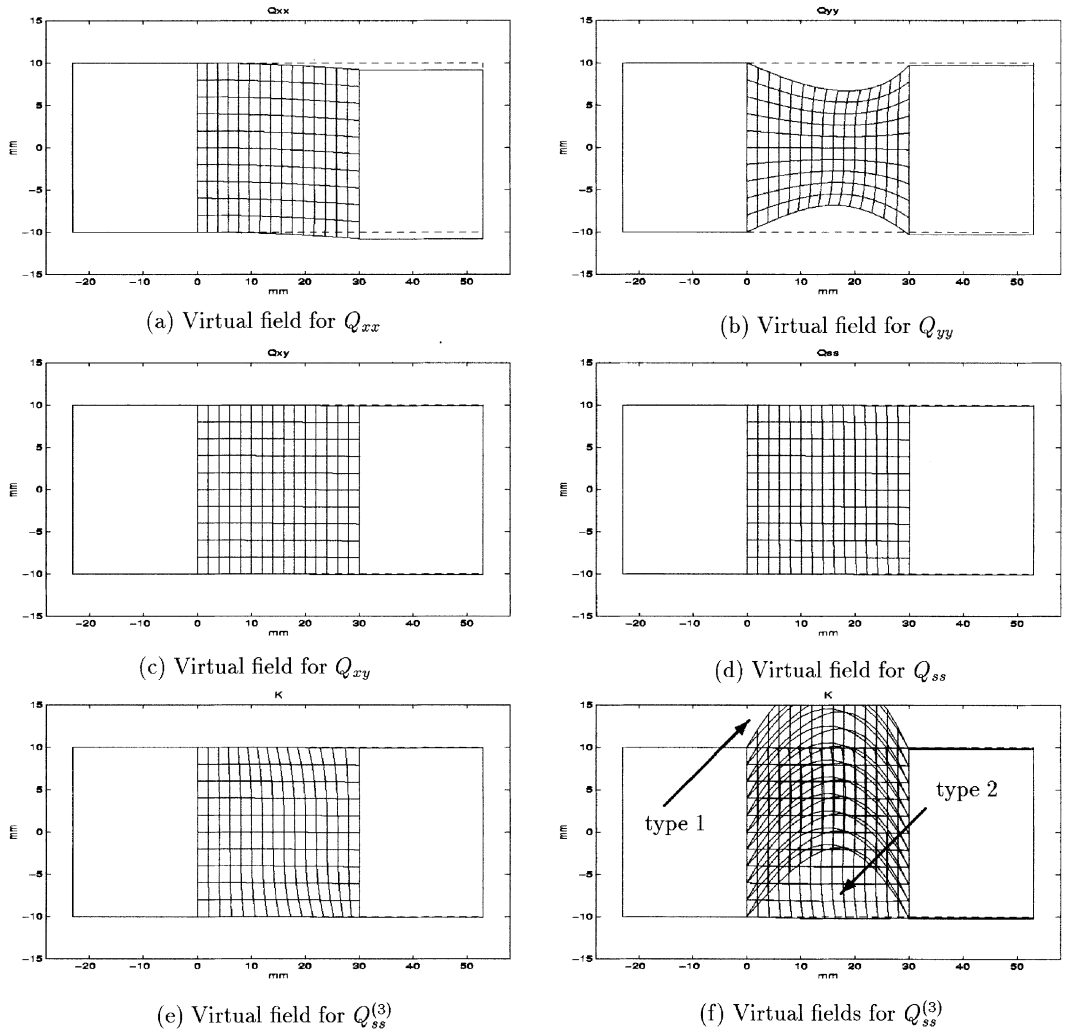

(a) Virtual field for Q_{xx}

(b) Virtual field for Q_{yy}

(c) Virtual field for Q_{xy}

(d) Virtual field for Q_{ss}

(e) Virtual field for $Q_{ss}^{(3)}$

(f) Virtual fields for $Q_{ss}^{(3)}$

Fig. 13. Optimized virtual fields, material 4, $p = 4\%$ and 12 first virtual fields obtained for $Q_{ss}^{(3)}$(f).

parameter is directly proportional to the difference between two non-zero values, since it was observed that the magnitude of these two coefficients was very close but their signs were opposite. Hence any slight variation of these two non-zero coefficients provides an important variation of the parameter to be identified. Eventually, this first type of virtual fields leads to unstable values for the unknown parameters. This is confirmed by the optimized virtual field in Fig. 13(e) which belongs to the second type of virtual fields. These five special virtual fields may be written as

$$\begin{cases} \hat{u}_x^{*(1)} = \frac{x(x-L)}{L^2}\left(0.789 - 3.61\frac{xy}{LH} - 1.26\frac{xy^3}{LH^3}\right) \times 10^5 \\ \hat{u}_y^{*(1)} = -0.398 \times \frac{x}{L} \times 10^5 \\ \hat{u}_x^{*(2)} = \frac{x(x-L)}{L^2}\left(0.054 + 0.45\frac{xy}{LH} - 2.70\frac{xy^3}{LH^3}\right) \times 10^5 \\ \hat{u}_y^{*(2)} = \frac{x}{L}\left(-0.014\frac{x}{L} - 0.844\frac{y}{H}\left(1 - \frac{x^2}{L^2}\right)\right) \times 10^6 \\ \hat{u}_x^{*(3)} = \frac{x(x-L)}{L^2}\left(3.51 - 0.461\frac{xy}{LH} - 0.16\frac{xy^3}{LH^3}\right) \times 10^5 \\ \hat{u}_y^{*(3)} = -0.051 \times \frac{x}{L} \times 10^6 \\ \hat{u}_x^{*(4)} = \frac{x(x-L)}{L^2}\left(0.03 - 1.12\frac{xy}{LH} + 6.66\frac{xy^3}{LH^3}\right) \times 10^5 \\ \hat{u}_y^{*(4)} = -0.059 \times \frac{x}{L} \times 10^3 \\ \hat{u}_x^{*(5)} = \frac{x(x-L)}{L^2}\left(-0.0176 - 0.65\frac{xy}{LH} + 3.85\frac{xy^3}{LH^3}\right) \times 10^5 \\ \hat{u}_y^{*(5)} = -0.006 \times \frac{x}{L} \times 10^6 \end{cases} \tag{36}$$

As can be stated, six monomials are used to build up the virtual fields, instead of five in the preceding cases. In the present case, 1, xy/LH, xy^3/LH^3 are used for u_x^* and x/L, y/H, x^2y/L^2H for u_y^*. The fact that the present results are presently more sensitive to noisy data than in the case of the linear response is in agreement with the above results. Indeed, the virtual fields are presently slightly more complicated (six monomials instead of five in the case of linearity) and it was observed in some previous studies that the number of monomials and the maximum power of their monomials were related to the stability of the results, as recalled above.

The present results are finally compared in a typical case to the parameters identified with a set of five virtual fields found intuitively (Grédiac et al., 2001) (see Table 7). It is clear that the present identified parameters are much more stable than the parameters found in Grédiac et al. (2001). This result confirms the relevance of the present approach.

Table 7
Identified parameters, material 4: Comparison with results obtained with virtual fields found intuitively (after Refs. Grédiac et al. (2001, 2002))

p (%)	Q_{xx} (GPa)	Q_{yy} (GPa)	Q_{xy} (GPa)	Q_{ss} (GPa)	Abs($Q_{ss}^{(3)}$) (GPa)
Reference	25.94	10.37	3.11	4.00	4420
Present work					
2	27.25	9.78	3.91	4.01	4116
	5.1%	−5.7%	25.7%	0.3%	−6.5%
Refs. Grédiac et al. (2001, 2002)					
$\frac{12}{512} \approx 2.3\%$	25.60	12.29	1.3	3.89	3665
	−1.3%	18.5%	−59.5%	−2.6%	−17%

5. Conclusion

The virtual fields method with special virtual fields allows a direct identification of parameters governing constitutive equations from heterogeneous strain fields. In this paper, the practical determination of the special virtual fields is carried out when the in-plane stiffnesses of orthotropic material are to be identified. Some numerical simulations have been carried to assess the feasibility, the accuracy and the stability of the method. The main conclusions are:

- Contrary to the procedure based on the updating of finite element models, the virtual fields method does not require any iterative calculations and the whole set of experimental points is taken into account: the input data is the actual field itself.
- The main improvement of the method here is to propose a procedure to find special virtual fields that *separately* provide the unknowns, i.e. independently one to the others.
- For each unknown, the special virtual fields behave like filters that extract the unknown from the measured actual virtual fields.
- These filters are presently chosen in such a way that only the central part of the actual strain field is processed. They can also eliminate some unknown information concerning the loading: for instance, only the resultant of the applied loading is considered, and not its distribution along the boundary of the grips.
- Each unknown mechanical parameter is equal to the virtual work produced by its associated special virtual fields.
- There exists an infinite number of special virtual fields per unknown parameters among which an optimized one is selected. The selection is based on the stability of the identified parameter to noisy data.
- The results of the simulations confirm the link between the stability of the results and the simplicity of the virtual fields in terms of number and degree of the monomials.

Some issues will be addressed in the near future:

- A parameter governing the non-linear shear response of a composite has been identified in the present work. This result is important and allows further developments in which parameters governing the damage of such materials can be identified.
- Coupling terms (either shear coupling terms or the stiffnesses that govern the in-plane/bending coupling) could also be determined with the present approach.
- Since the method is developed for specimens of any shape, it could be applied to other geometries and loading conditions for which the mechanical setup is simpler than the Iosipescu fixture.
- Polynomials were used to build up the virtual fields, but the suitability of other types of functions should be tested: sine or piecewise functions defined over the surface of the specimen to give more freedom to the virtual fields.
- It should also be relevant to find a simple criterion to obtain some information on the "identifiability" of the unknown parameters: it is clear that any identification method could not find a parameter which would not be involved in the actual stress/strain fields.

References

Araujo, A.L., Soares, C.M.M., Freitas, M.J.M., 1996. Characterization of material parameters of composite specimens using optimization and experimental data. Composites Part B 27 (2), 185–191.

Ayorinde, E., Gibson, R., 1993. Elastic constants of orthotropic composite materials using plate resonance frequencies, classical lamination theory and an optimized three-mode Rayleigh formulation. Composites Engineering 3 (5), 395–407.

Cerisier, F., 1997. Etude d'une transmission composite et de ses liaisons; Doctoral dissertation, University of Lyon, in French with English abstract.

Cunha, J., Piranda, J., 1999. Application of model updating techniques in dynamics for the identification of elastic constants of composite materials. Composites Part B 30, 79–85.

Deobald, L., Gibson, R., 1988. Determination of elastic constants of orthotropic plates by a modal analysis/Rayleigh-Ritz technique. Journal of Sound and Vibration 124 (2), 269–283.

Frederiksen, P.S., 1997. Numerical studies for identification of orthotropic elastic constants of thick plates. European Journal of Mechanics A/Solids 16, 117–140.

Grédiac, M., 1989. Principe des travaux virtuels et identification/principle of virtual work and identification. Comptes Rendus de l'Académie des Sciences, II/309:1–5. Gauthier-Villars, in French with Abridged English Version.

Grédiac, M., 1996a. On the direct determination of invariant parameters governing the bending of anisotropic plates. International Journal of Solids and Structures 33 (27), 3969–3982.

Grédiac, M., 1996b. The use of heterogeneous strain fields for the characterization of composite materials. Composite Science and Technology 56, 841–846.

Grédiac, M., Auslender, F., Pierron, F., 2001. Applying the virtual fields method to determine the through-thickness moduli of thick composites with a nonlinear shear response. Composites/Part A 32 (12), 1713–1725.

Grédiac, M., Pierron, F., 1998. A T-shaped specimen for the direct characterization of orthotropic materials. International Journal for Numerical Methods in Engineering 41, 293–309.

Grédiac, M., Pierron, F., Surrel, Y., 1999. Novel procedure for complete in-plane composite characterization using a T-shaped specimen. Experimental Mechanics 39 (2), 142–149.

Grédiac, M., Toussaint, E., Pierron, F., 2002. Special virtual fields for the direct determination of material parameters with the virtual fields method. 1—Principle and definition. International Journal of Solids and Structures, 39 (10), 2691–2705.

Grédiac, M., Vautrin, A., 1990. A new method for determination of bending rigidities of thin anisotropic plates. Journal of Applied Mechanics 57, 964–968.

Hendricks, M.A.N., 1991. Identification of the mechanical properties of solid materials. Doctoral dissertation, Eindhoven University of Technology.

Ho, H., Tsai, M.Y., Morton, J., Farley, G.L., 1994. Nonlinear numerical analysis of the Iosipescu specimen for composite materials. Composite Science and Technology 50, 355–365.

Mota Soares, C., Moreira de Freitas, M., Araújo, A.L., Pedersen, P., 1993. Identification of material properties of composite plate specimens. Composite Structures 25, 277–285.

Okada, H., Fukui, Y., Kumazawa, N., 1999. An inverse analysis determining the elastic–plastic stress–strain relationship using nonlinear sensitivities. Computer Modeling and Simulation in Engineering 4 (3), 176–185.

Pierron, F., Grédiac, M., 2000. Identification of the through-thickness moduli of thick composites from whole-field measurements using the Iosipescu fixture: theory and simulations. Composites: Part A 31 (4), 309–318.

Pierron, F., Vautrin, A., 1994. Accurate comparative determination of the in-plane shear modulus of t300/914 by the Iosipescu and 45° off-axis tests. Composite Science and Technology 52, 61–72.

Pierron, F., Vautrin, A., 1997. Measurement of the in-plane shear strength of unidirectional composites with the Iosipescu test. Composites Science and Technology 57 (12), 1653–1660.

Pierron, F., Zhavaronok, S., Grédiac, M., 2000. Identification of the through-thickness properties of thick laminates using the virtual fields method. International Journal of Solids and Structures 37 (32), 4437–4453.

Prabhakaran, R., Chermahini, R.G., 1984. Application of the least-squares method to elastic and photoelastic calibration of orthotropic composites. Experimental Mechanics 24, 17–21.

Swansson, S.R., Messick, M., Tombes, G.R., 1985. Comparison of torsion tubes and Iosipescu in-plane shear test results for a carbon epoxy composite. Composites 16 (3), 220–224.

Tsai, S., Hahn, H., 1980. Introduction to Composite Materials. Technomic.